JCTC Journal of Chemical Theory and Computation

Article

pubs.acs.org/JCTC

Surface Hopping Dynamics with Correlated Single-Reference Methods: 9H-Adenine as a Case Study

Felix Plasser,*[,†] Rachel Crespo-Otero,[‡,○] Marek Pederzoli,[§] Jiri Pittner,[§] Hans Lischka,[∇,⊥] and Mario Barbatti*[,‡]

[†]Interdisciplinary Center for Scientific Computing, Ruprecht-Karls-University, Im Neuenheimer Feld 368, 69120 Heidelberg, Germany

[‡]Max-Planck-Institut für Kohlenforschung, Kaiser-Wilhelm-Platz 1, D-45470 Mülheim an der Ruhr, Germany

[§]J. Heyrovský Institute of Physical Chemistry, Academy of Sciences of the Czech Republic, v.v.i., Dolejškova 3, 18223 Prague 8, Czech Republic

[∇]Department of Chemistry and Biochemistry, Texas Tech University, Lubbock, Texas 79409-1061, United States

[⊥]Institute for Theoretical Chemistry, University of Vienna, Währingerstr. 17, A-1090 Vienna, Austria

ABSTRACT: Surface hopping dynamics methods using the coupled cluster to approximated second order (CC2), the algebraic diagrammatic construction scheme to second order (ADC(2)), and the time-dependent density functional theory (TDDFT) were developed and implemented into the program system Newton-X. These procedures are especially well-suited to simulate nonadiabatic processes involving various excited states of the same multiplicity and the dynamics in the first excited state toward an energetic minimum or up to the region where a crossing with the ground state is found. 9H-adenine in the gas phase was selected as the test case. The results showed that dynamics with ADC(2) is very stable, whereas CC2 dynamics fails within 100 fs, because of numerical instabilities present in the case of quasi-degenerate excited states. ADC(2) dynamics correctly predicts the ultrafast character of the deactivation process. It predicts that C2-puckered conical intersections should be the preferential pathway for internal conversion for low-energy excitation. C6-puckered conical intersection also contributes appreciably to internal conversion, becoming as important as C2-puckered for high-energy excitations. In any case, H-elimination plays only a minor role. TDDFT based on a long-range corrected functional fails to predict the ultrafast deactivation. In the comparison with several other methods previously used for dynamics simulations of adenine, ADC(2) has the best performance, providing the most consistent results so far.

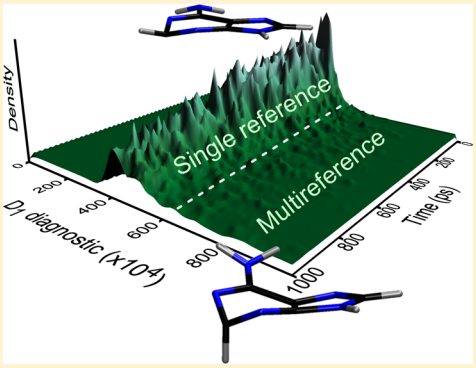

1. INTRODUCTION

Nonadiabatic dynamics has become a central method for the prediction of excited-state properties and the assignment of features in time-resolved spectra. However, the large computational cost of such simulations has led to the development of semiclassical independent-trajectory methods such as surface hopping,[1] as well as to the reduction of statistical ensembles[2] and the use of cost-effective low-level electronic structure methods.[3]

For many problems in photochemistry and photophysics, temporal evolution involves nonadiabatic relaxation through the manifold of excited electronic states of the same multiplicity until the minimum of the first excited state is reached (Kasha's rule) or until a region of crossing to the ground state of that multiplicity is found. For this early dynamics, static electron correlation of the ground state is often of minor importance for the description of the potential energy surfaces, compared with dynamic electron correlation. This motivates the search for single-reference methods that can be efficiently coupled to on-the-fly schemes for dynamics simulations. Time-dependent density functional theory (TDDFT) has been the method of choice for several groups recently,[4] and many successful cases have been published.[4c] (For a critical review on the applicability of different methods, see ref 3.) Sharing this motivation, in this work, we report the implementation of surface hopping dynamics based on different single-reference electronic structure methods. Specifically, we consider the second-order approximate coupled cluster (CC2)[5] and the algebraic diagrammatic construction to second order (ADC(2))[6] methods, which, in combination with the resolution of the identity (RI) approximation, can provide accurate potential energy surfaces at a computational cost that is feasible for on-the-fly dynamics simulations. While these two methods are very similar, from a methodological point of view, ADC(2) possesses the distinct advantage of being derived from a Hermitian eigenvalue problem, which increases the numerical stability of this method in the case of quasi-degenerate excited

Received: December 27, 2013
Published: February 28, 2014

   dx.doi.org/10.1021/ct4011079 | J. Chem. Theory Comput. 2014, 10, 1395−1405

states, as well as generally reducing the computational effort required for the computation of molecular properties and gradients. Surface hopping dynamics with CC2 and ADC(2) was implemented in an interface between the Netwon-X[7] and Turbomole[8] programs. In addition, we also present a new interface between Newton-X and Gaussian 09,[9] which extends the range of methods available to surface hopping dynamics to TDDFT with long-range corrected functionals[10] and Tamm-Dancoff approximation (TDA)[11] based either on restricted or unrestricted DFT.

Analytic nonadiabatic coupling vectors at the CC level have been considered only rarely in the literature,[12] and no implementation for either CC2 or ADC(2) is available. For this reason, and for the purpose of computational efficiency, we follow a different approach based on wave function overlaps of approximate configuration interaction with single excitations (CIS) wave functions. These overlaps may be used subsequently in connection with two algorithms for the propagation of the wave function: the standard adiabatic one,[13] and a locally-diabatic approach,[14] which was shown to be particularly stable in the case of highly peaked nonadiabatic couplings.[15] The procedures developed here certainly follow a pragmatic strategy, which, however, is expected to provide good results in cases where the ground-state wave function is well-described by a single determinant and the excited states by single excitations. In such circumstances, the changes in the character of the electronic wave function and nonadiabatic interactions will be computed fairly well. It should be kept in mind, at this point, that computational efficiency is a major criterion since, in the on-the-fly approach of surface hopping, excited-state energies and nonadiabatic interactions must be computed at each time step, leading to an extremely large computational effort.

We selected 9H-adenine in the gas phase to test these implementations. The advantage of working with this molecule for testing new methods is that results from dynamics simulations at several theoretical levels are available, including ab initio[16] and semiempirical[17] multireference configuration interaction (MRCI), semiempirical configuration interaction (CI) with floating-occupation molecular orbitals,[18] TDDFT with several functionals,[3,19] and time-dependent density functional tight binding (TD-DFTB).[20] Diverse dynamics methods have been used as well, including not only surface hopping,[3,16−18,20b] but also Ehrenfest dynamics[20a] and quantum wavepacket propagation.[19] Moreover, several experimental time-resolved spectra are also available in the gas phase.[21]

There is still another reason that makes it interesting to readdress the dynamics of 9H-adenine in the gas phase: although there is no doubt that 9H-adenine excited at the maximum of the first band returns to the ground state via internal conversion within ∼1 ps, there is no agreement about which reaction pathway is used. Simulations based on ab initio methods predicted that internal conversion occurs in a region of the seam of conical intersections characterized by puckering of the pyrimidine ring at the C2 atom (Figure 1).[16] However, other simulations based on semiempirical methods predicted that internal conversion happens at a C6-puckered region of the crossing seam.[17,18] Finally, other authors have suggested that the experiments indicate that H elimination from a NH bond is the actual way for internal conversion, even at low excitation energies.[21d]

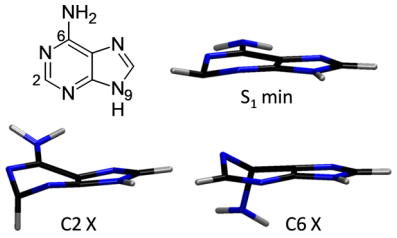

Figure 1. 9H-adenine structures of the S_1 minimum and of the C2 and C6 S_1/S_0 conical intersections (X).

2. COMPUTATIONAL DETAILS

Nonadiabatic dynamics was simulated with the fewest-switches surface hopping[1b] corrected for decoherence effects (α = 0.1 hartree).[22] Trajectories ran for a maximum of 1000 fs or until a S_1-S_0 energy gap smaller than 0.1 eV was reached. Integration was done with a time step of 0.5 fs for the classical equations and a time step of 0.025 fs for the quantum equations, using interpolated quantities between classical steps. The number of trajectories and the initial states are discussed later.

Electronic structure calculations were performed with CC2,[5] ADC(2),[6] and TDDFT.[23] CC2 is a simplification of the coupled-cluster singles and doubles (CCSD), which truncates the doubles equations such that excitation energies of singly excited states remain correct through second order in the fluctuation potential. Replacing double substitution amplitudes in the CC2 Jacobian $\mathbf{A}^{CC2}$ (a matrix in the space of single and double orbital substitutions) by their first-order approximations produces the Jacobian of the CIS(D_∞) approximation.[24] The ADC(2) method, which was originally derived using diagrammatic perturbation theory,[6a] may be expressed by the symmetric Jacobian $\mathbf{A}^{ADC(2)} = {}^1/_2(\mathbf{A}^{CIS(D\infty)} + \mathbf{A}^{CIS(D\infty)\dagger})$ where † indicates the conjugate transpose of $\mathbf{A}$. Excited-state energies of either of these approximations correspond to the eigenvalues of the respective Jacobian, while the contribution of each determinant to the excitation is associated to the eigenvectors.

Nonadiabatic interactions are computed during the dynamics by considering the numerical approximation proposed by Hammes-Schiffer and Tully.[13] In this approach, the inner product between the nonadiabatic coupling $\mathbf{F}_{kl}$ and the classical velocity $\mathbf{v}$ (both vectors in nuclear coordinate space) computed at time t is given by[15]

$$\mathbf{F}_{kl}\cdot\mathbf{v} \approx \frac{1}{4\Delta t}[3S_{kl}(t) - 3S_{lk}(t) - S_{kl}(t-\Delta t) + S_{lk}(t-\Delta t)] \quad (1)$$

where $S_{kl}(t)$ is the overlap integral of electronic wave functions ϕ_n for states k and l,

$$S_{kl}(t) = \langle\phi_k(t-\Delta t)|\phi_l(t)\rangle \quad (2)$$

and Δt is the integration time step. For TDDFT, this approximation has been successfully applied by several authors.[25] The wave function is written as a formal configuration interaction with single excitations (CIS) wave function:[26]

$$|\phi_n\rangle = \sum_{ia}\sqrt{\frac{\varepsilon_i - \varepsilon_a}{E_n}}X_{ia}^n|\Phi_{ia}\rangle \quad (3)$$

where $|\Phi_{ia}\rangle$ is a Slater determinant corresponding to an excitation from Kohn−Sham orbitals i to a with corresponding orbital energies ε_i and ε_a. E_n is the excitation energy for state n.

dx.doi.org/10.1021/ct4011079 | J. Chem. Theory Comput. 2014, 10, 1395−1405

Table 1. Characterization of the First Absorption Band of 9H-Adenine

	RI-CC2		RI-ADC(2)		TD-ωB97XD		Experiment[a]	
	ΔE (eV)	f	ΔE (eV)	f	ΔE (eV)	f	ΔE (eV)	f
n−π*	5.08	0.021	5.00	0.026	5.33	0.001		
π−π*	5.13	−0.034	5.06	0.169	5.33	0.280	5.16 ± 0.07[b]	0.24[c]
π−π*	5.16	0.300	5.07	0.101	5.46	0.012		
π−3s	5.39	0.013	5.39	0.010	5.88	0.006		
band maximum	4.95		4.87		5.09		5.07,[d] 4.92[c]	
fwhm/σ^{max}[e]	0.57	0.534	0.62	0.497	0.59	0.501	0.55[c]	0.463[c]

[a]Experimental results obtained in vapor. [b]Data taken from ref 32. [c]Data taken from ref 33a. [d]Data taken from ref 33b. [e]fwhm represents the full width at half maximum; σ^{max} is defined as the maximum of the absorption cross section (in Å^2 molecule^{-1}).

X^n_{ia} is the time-dependent linear-response pseudo-eigenvector for the same determinant for state n. In the construction of the wave function, the Y^n_{ia} components of the pseudo-eigenvector are neglected and X^n_{ia} are orthogonalized, implying that the nonadiabatic couplings are computed within an approach equivalent to the Tamm−Dancoff approximation.

Similarly, for CC2, an approximate wave function is constructed as

$$|\phi_n\rangle = \sum_{ia} R^n_{ia}|\Phi_{ia}\rangle \quad (4)$$

$$\langle\phi_n| = \sum_{ia} L^n_{ia}\langle\Phi_{ia}| \quad (5)$$

where R^n_{ia} and L^n_{ia} are the single substitution parts of the right and left Jacobian eingenvectors. For ADC(2), the same expression is used with $L^n_{ia} = R^n_{ia}$. From these CIS wave functions built at two sequential time steps, the wave function overlaps (eq 2) are computed as described in refs 25c and 27.

To arrive at eqs 4 and 5, several approximations that rely on the predominance of single excitations in the wave function are introduced. These approximations allow for an efficient computation of the overlap matrix elements. First, doubles amplitudes are neglected, because they are never explicitly stored in the Turbomole implementation[5b] of CC2 and ADC(2), which exploits the diagonality of the double/double blocks of the Jacobian to reformulate the eigenvalue problem in the single-substitution space only. For simplicity reasons, the singles amplitudes are used to construct a formal CIS wave function, rather than an actual CC wave function. Per default, these truncated wave functions are reorthonormalized (see ref 12c with regard to challenges in normalizing the original CC wave functions). In addition, in the case of CC2, where right and left eigenvectors are different (forming a biorthogonal system) due to the nonsymmetry of the Jacobian, we compute the overlap of the right vectors of the respective current time step with the left vectors from the previous one. These approximations allow us to compute the overlaps at a reasonable effort (∼20% of the total computation time for one single step). By contrast, one would expect the exact overlaps of CC wave functions to scale exponentially with system size, and, to our knowledge, such calculations have never been attempted.

A ground-state harmonic-oscillator Wigner distribution for the nuclei was used to simulate the absorption spectrum with the Nuclear Ensemble (NE) approach.[28] The parameters for the spectrum simulations were N_p = 500 (number of ensemble points), N_{fs} = 6 (number of excited states), and δ = 0.1 eV (Gaussian line broadening). Initial conditions for dynamics were obtained from the absorption spectrum in restricted spectral domains, as explained later in section 3.2.

Turbomole was used for CC2 and ADC(2) calculations, and Gaussian 09 was used for TDDFT. Newton-X interfaced to these programs was used for dynamics simulations. In the cases of TDDFT, trajectories were computed with the long-range and dispersion corrected ωB97XD functional.[10,29] To the best of our knowledge, this is the first study using long-range corrected functionals in combination with surface hopping dynamics. The aug-cc-pVDZ basis set[30] was adopted for all calculations.

For comparison, nonadiabatic coupling vectors were computed at the multireference configuration interaction level with single excitations (MR-CIS) using the aug-cc-pVDZ basis set, based on a complete active reference space of 10 electrons in 8 orbitals (3π, 2n, 3π*). These orbitals were generated using a complete active space self-consistent field calculation in the same active space. These computations were performed with the Columbus program package.[31]

3. RESULTS

3.1. Vertical Excitations and S_1 Minimum. The vertical excitation energies into the lowest singlet states of 9H-adenine are given in Table 1. The lowest excitation is into the n−π* state, which is closely followed by two π−π* states and then by the Rydberg π−3s. The experimental value for the vertical excitation was proposed in ref 32, based on vapor spectra of adenine reported in ref 33. It was estimated by adding the deviation between the computed vertical excitation and the simulated band maximum to the experimental band maximum.[32] The comparison of the computational values with the experimental result for the π−π* states is excellent for all methods. The CC2 energies fall within the experimental error bar, while the ADC(2) result is lower than the experiment by 0.1 eV. CC2 results with aug-cc-pVTZ basis set reported in ref 34 are ∼0.1 eV larger than those in Table 1. It may also be noted that the hierarchically superior EOM-CCSD(T) method puts the dark n−π* states somewhat above the π−π* states, changing the state ordering.[35] With TDDFT, the vertical excitations of adenine are rather sensitive to the functional, as we have discussed previously.[3] Specifically, for ωB97XD, the vertical excitation energy is 0.17 eV higher than the experimental value. For all methods, there are substantial Rydberg contributions to the π−π* states. The combined oscillator strengths of the π−π* states are slightly larger than the experimental value. The negative oscillator strength in CC2 reflects the imaginary root arising from the quasi-degeneracy of the states.[34]

Because of the close energy spacing between the π−π* states, mixing between them is quite strong, resulting in significant

discrepancies for the oscillator strengths of the adiabatic S_1 and S_2 states between the different methods presented in Table 1. For comparison to the experiments, however, the quantity that matters is the total oscillator strength of the two $\pi-\pi^*$ states, rather than their individual values. Furthermore, these values are also strongly geometry-dependent. These conditions pose challenges for a proper choice of initial states. Our solution to this problem is described in section 3.2: the initial state is probabilistically chosen according to the oscillator strength at the respective geometry. In other words, the states with strong oscillator strengths are chosen irrespective of the adiabatic ordering.

CC2 and ADC(2) predict the S_1 minimum of adenine with an envelope conformation (^{2}E) puckered at C2 (Figure 1). The minimum is of $n-\pi^*$ nature, but is strongly mixed with $\pi-\pi^*$ character. According to the experiments conducted in water,[36] the weak luminescence of adenine (quantum yield 2.6×10^{-4}) is peaked at 3.86 eV with a shoulder at 3.00 eV. Our investigations in the gas phase did not show any evidence of an energy minimum with a gap as large as 3.86 eV to the ground state. However, both methods show the existence of a flat region on the S_1 surface ($n-\pi^*$) with a barrierless connection to the S_1 minimum (see also ref 37). This flat region corresponds to planar geometries, and it is 3.7 eV (3.6 eV) above the ground state, according to CC2 (ADC(2)). This could imply that either CC2 and ADC(2) do not properly describe a small barrier separating the flat region from the puckered minimum or that this small barrier is ultimately caused by interaction of 9H-adenine with water. In any case, the correspondence between CC2 and ADC(2) emission energies (3.10 and 2.96 eV, Table 2) and the experimental shoulder at 3.00 eV is once more remarkable. The adiabatic excitation energy is 4.42 eV at CC2 and 4.29 eV at ADC(2). These values are also in good agreement with the resonant two-photon ionization (R2PI) measurements of adenine vapor, which established the band origin to be in the 4.40–4.47 eV region.[38] In comparison, CASSCF optimization of 9H-adenine shows two minima: one planar and one puckered.[39] The energy barrier connecting them (starting from the highest minimum) is only 0.12 eV at CASPT2 level, using the CASSCF geometries. It is not clear at this point whether the inclusion of dynamic electron correlation in the optimization would eliminate or enhance this barrier.

Table 2. Characterization of the S_1 Minimum Optimized with CC2, ADC(2), and TD-ωB97XD (aug-cc-pVDZ) in Terms of the Vertical Excitation Energy (ΔE), Adiabatic Excitation Energy (ΔE_a), and Cremer–Pople Parameters

	CC2	ADC(2)	TD-ωB97XD	experiment
ΔE (eV)	3.10	2.96	3.98	3.86, 3.00[a]
ΔE_a (eV)	4.42	4.29	4.68	4.40–4.47[b]
ϕ (°)	246	246		
θ (°)	121	121		
Q (Å)	0.26	0.27	0.00	
Conform.	^{2}E	^{2}E	planar	

[a]Fluorescence band maximum and shoulder in water (pH 7.3); data taken from ref 36. [b]R2PI band origin (gas phase); data taken from ref 38.

TD-ωB97XD predicts the existence of a planar S_1 minimum with $n-\pi^*$ character and an emission energy of 3.98 eV. Every attempt of optimizing a puckered minimum ends up back at that planar minimum. This situation is similar to that observed with other functionals[3] and, curiously, it is exactly the opposite of the CC2 and ADC(2) results discussed above, where a puckered minimum was found, but not a planar one.

3.2. Absorption Spectrum and Initial Conditions. The absorption spectrum of 9H-adenine was simulated using the NE approach, which provides intensities and band widths in absolute units (although without vibrational resolution).[28] The results are shown in the top portion of Figure 2, together with the experimental results from ref 33a (see ref 40, too). The CC2 band maximum (4.95 eV, Table 1) is in excellent agreement with the vapor spectrum measured by Clark et al.[33a] (4.92 eV). The ADC(2) maximum (4.87 eV) is slightly red-shifted, when the same experiments are compared to each other. The TD-ωB97XD maximum is blue-shifted by 0.17 eV, which, remarkably, is the same shift observed in the vertical excitation. The experimental and simulated full widths at the half-maximum (fwhm) agree within 0.05 eV. The simulated maximum of the absorption cross section is larger than the experimental measurement by 0.07 Å^2 molecule^{-1} for CC2, 0.03 Å^2 molecule^{-1} for ADC(2), and 0.04 Å^2 molecule^{-1} for TD-ωB97XD (see Table 1).

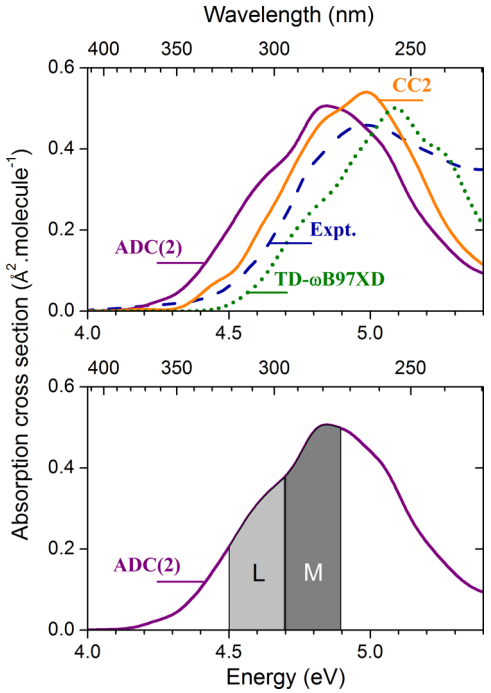

Figure 2. Absorption spectrum of 9H-adenine. Top panel shows results for CC2, ADC(2) and TD-ωB97XD simulations (experimental results obtained in vapor).[33a] Bottom panel presents the ADC(2) spectrum, showing the L (4.6 ± 0.1 eV) and M (4.8 ± 0.1 eV) domains from where initial conditions for dynamics were selected.

For ADC(2), initial conditions for dynamics were sampled from two domains in the simulated spectra: L (low) and M (medium). The L-domain is defined as residing in the 4.6 ± 0.1 eV range, whereas the M-domain is defined as residing in the 4.8 ± 0.1 eV range (bottom panel of Figure 2). From the initial $N_p \times N_{fs} = 500 \times 6 = 3000$ spectral points used to build the spectrum, 218 points are in the L-domain and 407 points are in the M-domain. Each point corresponds to a set of random nuclear geometry and velocity given by the Wigner distribution. The M-domain was selected to approximately emulate the

experimental pump at 251.3 nm (4.93 eV),[21e] corresponding to the band maximum. The L-domain was selected to emulate the pump at 265.1 nm (4.68 eV),[21e] which is the middle of the low-energy side of the absorption band.

To select initial conditions from each of these domains, the photoexcitation probability is computed for each point in the domain. This probability is given by the oscillator strength of the point normalized by the maximum oscillator strength in the ensemble. Then, a stochastic algorithm selects points within the domain according to this probability. After this screening, 61 points were selected in the L-domain (Table 3): 45 correspond to excitations into S_1, 13 into S_2, and 3 into S_3. As we limited our simulations to 50 trajectories in each domain, to keep the same proportion of points being excited into each state, 38 trajectories were started in S_1, 12 in S_2 state and none in S_3. With the same selection procedure for the M-domain, we started 14 trajectories in S_1, 32 in S_2, and 4 in S_3.

Table 3. Number of Spectral Points and of Initial Conditions in the L- and M-Domains for ADC(2) Simulations

domain (eV)		S_1	S_2	S_3	S_4	total
4.6 ± 0.1 (L)	spectrum	45	13	3	0	61
	trajectories	38	12	0	0	50
4.8 ± 0.1 (M)	spectrum	34	75	10	1	120
	trajectories	14	32	4	0	50

3.3. Dynamics. *3.3.1. Suitability of ADC(2) and CC2 for Dynamics.* Dynamics with CC2 was tested with a set of 10 trajectories initiated in the 4.7 ± 0.1 eV domain. All of them failed due to numerical problems within the first 100 fs. This happened because of the nonsymmetric CC2 Jacobian, which tends to produce imaginary eigenvalues (energies) near degenerated excited states.[24]

ADC(2) does not show this problem because it has a symmetric Jacobian, whose eigenvalues are always strictly real. Dynamics with this method was perfectly stable and trajectories ran until one of the termination criteria was achieved. In terms of computational time, 2000 steps for 1 ps trajectory computed with RI-ADC(2)/aug-cc-pVDZ, 3 excited states, required ∼24 days running on 4 cores of a 2.7 GHz Xeon processor. This computational demand may, in principle, be alleviated by restricting the virtual space as discussed in ref 41, but this feature was not tested in this work.

The reliability of ADC(2) calculations may be estimated by computing the D_1 and D_2 diagnostics.[42] The D_1 diagnostic[42a] measures the interaction between the Hartree−Fock (HF) reference state and singly-excited determinants. High D_1 values indicate multireference character of the ground state. The D_2 diagnostic[42b] measures the interaction between the HF reference and doubly-excited determinants, thus, high values indicate large contributions of double excitations for the excited state in question.

The initially recommended values for D_1(MP2) and D_2(CCSD) are $D_1 < 0.04$ and $D_2 < 0.17$.[42] Even though adenine has D_1(MP2) and D_2(ADC(2)) above the recommended thresholds already in the ground-state minimum (0.042 and 0.26, respectively), all our tests indicated that ADC(2) provides a good description of the lowest electronic states of adenine. This seems to imply that the recommended values, obtained for MP2 and CCSD ground-state calculations on a benchmark of small molecules (no aromatic systems included), establish a safety margin that is too narrow to account for molecules such as 9H-adenine. In fact, based on the evaluation of excited states computed with CC2 for a set of

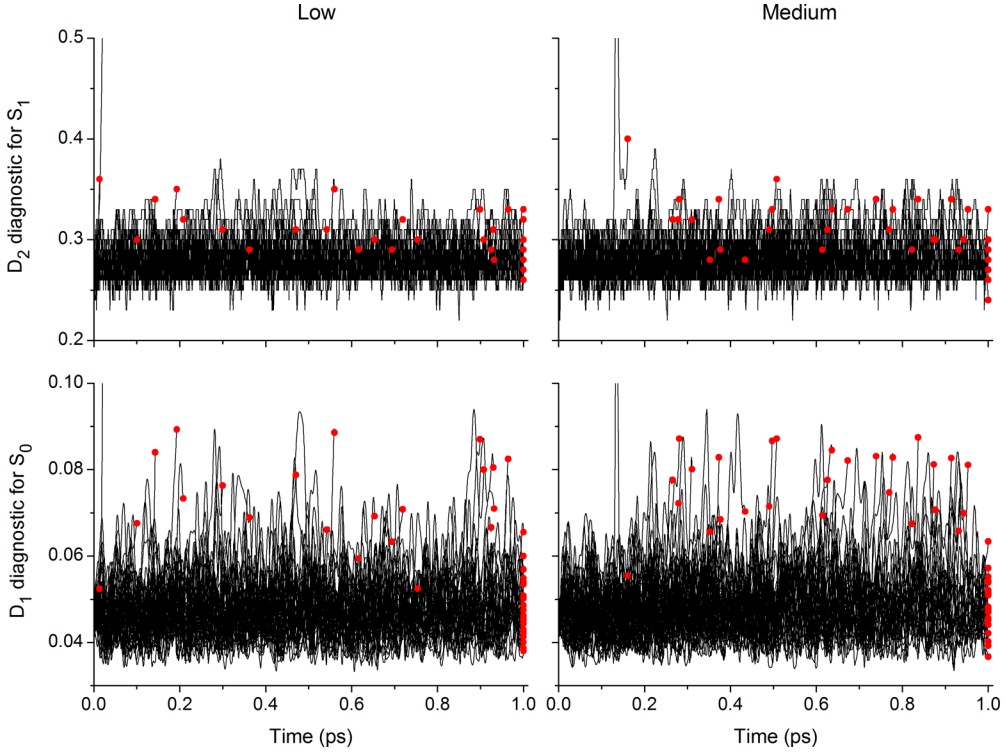

Figure 3. D_1(MP2) diagnostic for the ground state and D_2(ADC(2)) diagnostic for S_1 along the dynamics. Dots indicate the values at the last point of each trajectory.

dx.doi.org/10.1021/ct4011079 | J. Chem. Theory Comput. 2014, 10, 1395−1405

molecules, Köhn and Hättig concluded that D_1 values up 0.15 and D_2 values up to 0.25 are still acceptable.[43]

D_1(MP2) and D_2(ADC(2)) diagnostics along the dynamics are shown in Figure 3 for all trajectories. Most of time, D_1 is between 0.04 and 0.06. Intersections with the ground state are found with D_1 between 0.06 and 0.09, reflecting the strong multireference character of the ground state in such cases, as expected. D_2 for S_1 is mostly between 0.25 and 0.35. Intersections with the ground state are found for D_2 in the upper region of this domain, indicating some contribution from double excitations near the crossing.

The exceptional numerical stability of the ADC(2) method manifested itself in the fact that, if the termination criteria are not applied, trajectories continue running with formal negative excitation energies (response state lower than the closed shell) after S_1−S_0 crossings. However, note that the ADC(2) method is not able to treat this area of low S_1−S_0 gaps properly. In this area, there should be strong mixing between the closed shell and the excited configurations, which is absent in the single reference treatment. Thus, ADC(2) cannot be expected to be able to properly represent the two-dimensional (2D) branching space for S_1−S_0 crossings, just as this is the case for CIS and TDDFT (in its linear response formalism based on the adiabatic approximation).[44] Therefore, we want to stress that ADC(2) cannot describe the details of the deactivation process to the ground state. If information about the precise deactivation geometry is required or if the dynamics is to be continued in the S_0 state (as is the case, for example, when computing isomerization quantum yields), then ADC(2) is certainly not the method of choice and we suggest using one of the multireference methods, which are already available within Newton-X. However, if, as in the present case of adenine, we are interested in excited-state lifetimes or in the general deactivation pathways used, we can simulate the dynamics until a small energy gap to the ground state is reached. This provides approximately a lower limit for the excited-state lifetime and reliable distribution of excited-state pathways. Even more, if a fluorescent species is considered or if the primary interest lies in processes happening within the excited state manifold, ADC(2) (and, similarly, TDDFT with a properly chosen functional) may indeed be the efficient and reliable method of choice.

3.3.2. Numerical Test of the Coupling Elements. Before presenting the results of the dynamics simulations, we will discuss the reliability of the coupling elements as computed with the methodology described above. Unfortunately, no analytic coupling terms are available at the ADC(2) level. Therefore, we resort to MR-CI, for which analytical coupling vectors are implemented.[45] Specifically, we use MR-CIS out of a CAS(10,8) reference space, using the same aug-cc-pVDZ basis set used for the ADC(2) calculations. When performing this comparison, one should remember that differences will not only be derived from the approximations in the ADC(2) coupling elements, but also simply from differences in the wave function descriptions of the ADC(2) and MR-CIS methods. For this reason, a systematic evaluation is difficult and we will limit ourselves to the discussion of one exemplary trajectory (see Figure 4). This trajectory was chosen as a rather challenging case, showing two surface hops within a time window of 10 fs.

In the original ADC(2) trajectory (Figure 4, open circles (○)) there was a surface hop from S_1 to S_2 at 143.0 fs after photoexcitation, quickly followed by a second hop to S_1 at 148.5 fs. The first hop was initiated by a small decrease in the

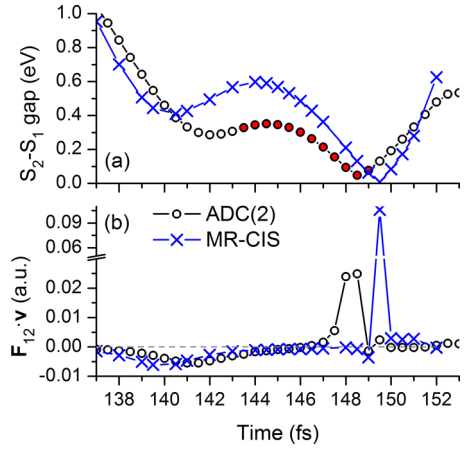

Figure 4. Comparison of the ADC(2) and MR-CIS methods for adenine, using a given ADC(2) trajectory: (a) energy gap between the first two excited states (solid red circles (●) mark times when the system is in the S_2 state) and (b) nonadiabatic coupling elements.

S_2−S_1 energy gap (0.287 eV), accompanied by a modest $\mathbf{F}_{12}\cdot\mathbf{v}$ coupling element (as defined in eq 1) spread out over a few femtoseconds, reaching a maximum of −0.0055 a.u. at 141.5 fs. In the case of the second hop, the energy gap was significantly reduced (0.048 eV), which coincided with a strong positive coupling reaching up to 0.025 a.u., lasting for only two time steps.

To evaluate the reliability of these outcomes, we recomputed the same trajectory at the MR-CIS level. For this purpose, nonadiabatic coupling vectors $\mathbf{F}_{12}$ were evaluated at the geometries determined from ADC(2) and the $\mathbf{F}_{12}\cdot\mathbf{v}$ terms were explicitly computed with respect to the instantaneous velocities also derived from the ADC(2) trajectory. The results are presented as blue crosses (×) in Figure 4. The overall trends are very similar to ADC(2): In the first part, there is a lowering of the S_2−S_1 gap, accompanied by a moderate coupling (reaching up to −0.0061 a.u., already at 139.5 fs). In the second part, there is a more weakly avoided crossing with a positive $\mathbf{F}_{12}\cdot\mathbf{v}$ element. As opposed to the ADC(2) calculations, the trajectory reaches a point, which is very close to the MR-CIS crossing seam (with an energy gap of 0.007 eV at 149.0 fs). This is accompanied by a highly peaked coupling element at the same time step (reaching a value of 0.106 a.u.).

In summary, one can say that the approximate ADC(2) couplings reproduced the results obtained with analytical MR-CIS coupling vectors in a semiquantitative way. Using the current implementation, even phase changes in the coupling elements can be readily identified, thus providing a good description of cases where multiple nonadiabatic events occur in close succession. Differences between the coupling elements (Figure 4b) correlate with energetic differences (Figure 4a), showing that these are, for the most part, derived from general differences between the ADC(2) and MR-CIS methods, rather than specifically from our approximation protocol.

3.3.3. Results of the ADC(2) Dynamics. Surface hopping trajectories were computed for a maximum of 1000 fs or until a S_1−S_0 energy gap smaller than 0.1 eV was reached. Initially, 24% of the trajectories are in S_2 in the L-domain and 72% are in either S_2 or S_3 in the M-domain (see Table 3). This highly excited population deactivates to S_1 within 60 fs in the L-domain and 54 fs in the M-domain. After that, small population

dx.doi.org/10.1021/ct4011079 | J. Chem. Theory Comput. 2014, 10, 1395−1405

fluctuations between S_1 and S_2 are observed along the dynamics.

In the cases that a small energy gap to the ground state was reached, we assumed that internal conversion to the ground state took place. The fraction of trajectories returning to the ground state within 1 ps, according to this criterion, is given in

Table 4. Fraction of Trajectories Returning to the Ground State within 1 ps

	Fraction of Trajectories	
	L-domain	M-domain
S_1	0.61	0.64
S_2	0.17	0.55
S_3		0.50
total	0.50 ± 0.12	0.57 ± 0.12
expt[a]	0.62 ± 0.02	0.68 ± 0.02

[a]Data taken from ref 21e.

Table 4. The margins of error for the deactivation yields were computed using the expression[46]

$$\varepsilon = Z\sqrt{\frac{p(1-p)}{N}} \tag{6}$$

where p is the deactivation probability, N is the number of trajectories, and $Z = 1.6449$ for a 90% confidence interval.

Half of trajectories in the L-domain returned to the ground state. In the M-domain, 57% returned to the ground state. Assuming a simple exponential decay, we can use the experimental lifetimes[21e] after pumping at 265.1 nm (L) and 251.3 nm (M) to estimate that 62% and 68% of the population, respectively, should be in the ground state within 1 ps. This means that ADC(2) estimates of the deactivation are somewhat smaller than the experimental values.

With 50 trajectories, the margin of error in the estimate of the deactivation is ±12% for a 90% confidence level. This implies, first, that the increase of the deactivation from L to M is not statistically significant. Second, the small level of deactivation predicted by ADC(2) compared with the experiment, although still within the limit of the statistical error, may indicate that ADC(2) is, in fact, overestimating the excited-state lifetime.

The distribution of trajectories in the space of the Cremer–Pople parameters[47] (Q, θ, and ϕ) is shown in Figure 5. There is no substantial distinction between trajectories in the L- and M-domains. Averaging over all time steps and trajectories, the degree of puckering (Q) in the pyrimidine ring is 0.22 Å for both domains, which is slightly smaller than the 0.27 Å observed at the S_1 minimum (see Table 2). The Q-distribution is very asymmetric, with almost no geometries near 0 Å (planar pyrimidine ring), and a long tail extending to Q as large as 0.7 Å. Intersections to the ground state are reached for $Q = 0.5 \pm 0.1$ Å.

The type of puckering deformation in the pyrimidine ring is given by the parameters θ and ϕ.[48] Trajectories cluster in two regions of this space corresponding to the ^{2}E (envelope conformation with C2 above the ring plane) and E_2 (envelope with C2 below the plane). Crossings to the ground state are found not only at these C2-puckered regions, but also at C6-puckered regions (for instance, around $\theta = \phi = 120°$). These deformations are related to the two types of puckered conical intersections shown in Figure 1.

The fractions of C2-puckered, C6-puckered, and N–H stretched geometries used for internal conversion to the ground state are given in Table 5. For the L-domain, internal conversion happens mainly through C2 deformations, but also C6 deformations play a considerable role. The importance of internal conversion through C6 increases in the M-domain, practically equaling C2, reflecting the larger amount of available energy. In both domains, N–H elimination is much more rare.

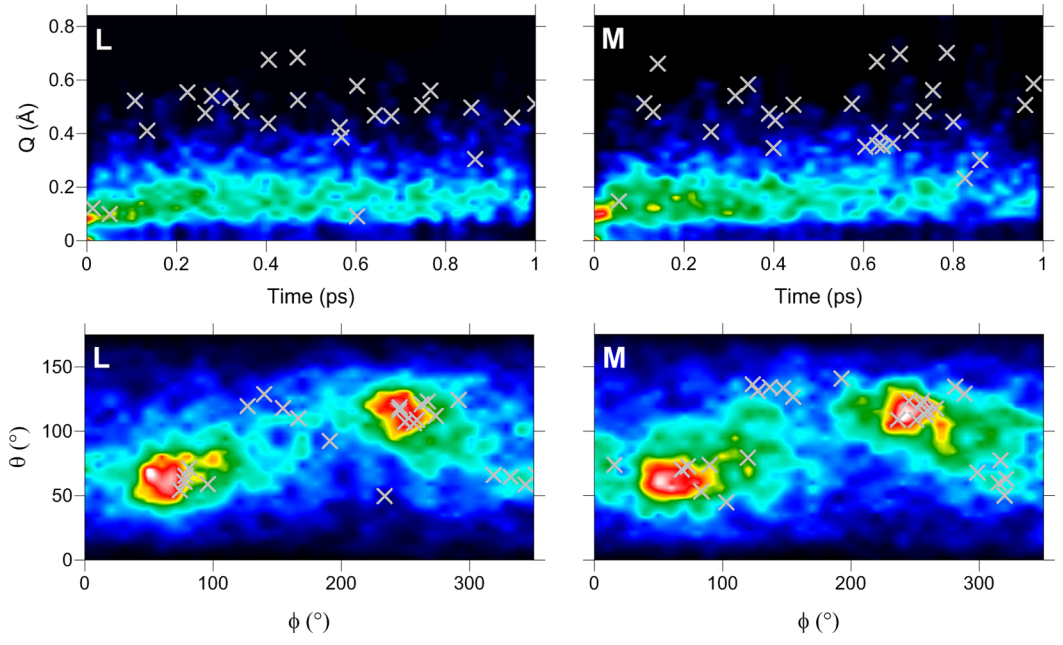

Figure 5. Distribution of Cremer–Pople parameters during the dynamics. Red regions indicate larger densities than black regions. The crosses indicate the smallest energy gap to the ground state ($\Delta E_{12} < 0.1$ eV) when trajectories are stopped.

dx.doi.org/10.1021/ct4011079 | J. Chem. Theory Comput. 2014, 10, 1395–1405

Table 5. Fraction of Trajectories Returning to the Ground State in Each of the Three Main Deactivation Channels

	Fraction of Trajectories	
	L-domain	M-domain
C2	0.52	0.54
C6	0.36	0.43
H-elimin.	0.12	0.03

To help rationalize these results, ADC(2) energy profiles were computed with linear interpolation of internal coordinates (LIIC) between the S_0 minimum and the S_1 minimum, and then between the S_1 minimum and the conical intersections (Figure 6). Although LIIC tends to overestimate reaction

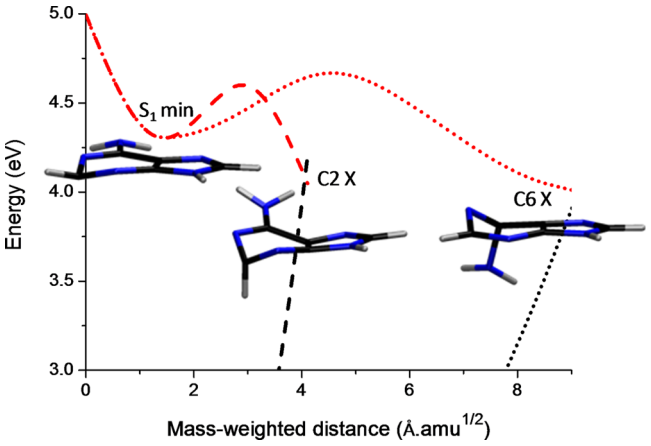

Figure 6. LIIC energy profiles of the ground and first excited states from the S_0 minimum to the S_1 minimum and then to the C2 and C6 conical intersections (X) computed with ADC(2).

barriers, it usually reflects the general features of the reaction paths well, especially when computed with natural internal coordinates,[49] as done here. The reaction barrier to move from the S_1 minimum to the C2 conical intersection is slightly smaller than that to move to the C6 intersection by 0.08 eV. Moreover, the barrier to C2 is much closer to the S_1 minimum than the barrier to C6. Thus, energetic factors (barrier height) and, especially, entropic factors (barrier distance) favor adenine to move toward C2 intersection rather than to C6 intersection. This is an indication that the slight predominance of C2 deformations (Table 5) may persist, even for a more statistically significant ensemble of data.

3.3.4. Comparison among Methods. In a previous work,[3] we reported dynamics simulations of 9H-adenine with several different methods, including ab initio and semiempirical versions of multireference configuration interaction (MR-CIS and OM2/MRCI, respectively), and TDDFT with several functionals. The predicted S_0 populations at 1 ps for the M-domain are shown in Figure 7, together with the experimental result from ref 21e. We found out that excited-state lifetimes and distribution of reaction pathways could be significantly different among the methods, because of the quality of the potential energy surfaces.

The ultrafast deactivation of adenine is predicted to occur at deactivation rates comparable to experiment at ADC(2), OM2/MRCI, and MR-CIS levels, although MR-CIS overshoots the rate somewhat. No matter the functional, the deactivation level predicted by TDDFT is far too low, even taking into account

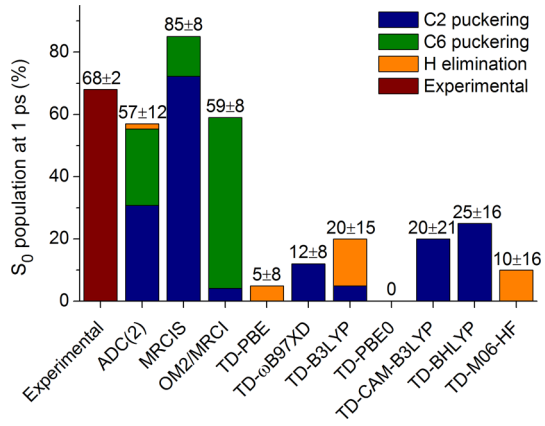

Figure 7. Comparison of the present ADC(2) results for deactivation within 1 ps with the experimental[21e] and diverse computational[3] results. The TD-ωB97XD result is also reported here for the first time. Margins of error estimated for a 90% confidence level.

the large margins of errors that are due to the small trajectory samples. With OM2/MRCI, deactivation occurs mostly at C6 deformed geometries, whereas with MR-CIS, it occurs mostly at C2 deformed ones. With ADC(2), deactivation occurs mainly at C2 deformation, but with considerable contribution of C6. In ref 3, it has been shown that better balanced active and reference spaces increase the participation of C6 deformed geometries in MR-CIS dynamics, bringing it closer to the ADC(2) result.

TDDFT with the ωB97XD functional, which is reported here for the first time, followed the same pattern that has been observed with other functionals discussed in ref 3. Fifty (50) trajectories—30 starting in S_2 and 20 in S_3—were simulated, sampling the entire first spectral band. The deactivation level was very small and only 6 trajectories (12%) returned to ground state within 1 ps. For all 6 of these trajectories, C2 deformations are responsible for the energy crossing, which is also consistent with the previous TDDFT results for other functionals. As we have discussed in ref 3, the failure of TDDFT to describe the excited-state dynamics of adenine is related to the DFT overstabilization of the ground-state potential energy along planar distortions, compared to out-of-plane distortions. This effect creates a bias toward motion with small degree of puckering, delaying the time to reach the conical intersections.

Even though ADC(2) and OM2/MRCI predict similar S_0 populations (Figure 7), potential energy profiles computed at these and higher levels of theory[3] indicate that ADC(2) results should provide the best results. Compared with CC2 and CASPT2 profiles (see Figure 4 of ref 3), OM2/MRCI clearly underestimates the reaction barrier between the S_1 minimum and the C6-puckered conical intersection. This not only explains the high number of hops at C6-puckered geometries, but also indicates that OM2/MRCI may be predicting the right excited-state lifetime in part for the wrong reason. ADC(2), in turn, has potential energy profiles that compare very well to the high-level calculations (compare Figure 6 with Figure 4 of ref 3).

One question that remains is why the S_0 population predicted by ADC(2) (57% ± 12%) is smaller (at a significance level of 0.1) than the experimental result (68% ± 2%). Although we would need better statistical samples to clarify this point, we want to briefly discuss possible reasons for this

dx.doi.org/10.1021/ct4011079 | J. Chem. Theory Comput. 2014, 10, 1395−1405

discrepancy. This, of course, could be an indication of a methodological shortcoming, e.g., that ADC(2) is not properly describing the potential energy surface of the lowest excited state of adenine. We may also point out that other elements may partially account for the divergence. First, the simulations included only the 9H tautomer, whereas the experiment may have appreciable amounts of the 7H tautomer. Another source of divergence is that, while the simulations are really providing the S_0 population at 1 ps (or with the present methodology at least an upper bound to it), the experimental value corresponds to the fitting of the transient absorption spectrum, which includes information of the ionization process during the probing.[21f,32]

4. CONCLUSIONS

Nonadiabatic surface hopping dynamics was implemented based on on-the-fly electronic structure calculations with the CC2 and ADC(2) methods available in the Turbomole program. The implementation of surface hopping based on TDDFT available in Gaussian 09 also is reported. For all cases, nonadiabatic couplings are based on overlaps of formal CIS wave functions. In practical terms, dynamics can be performed only with ADC(2) and TDDFT, which do not suffer from the instabilities near degenerate excited states observed in methods with nonsymmetrical Jacobians.

As a common limitation of a single-reference method, internal conversion to the ground state cannot be simulated with ADC(2), although it is possible to follow the nonadiabatic dynamics involving several excited states until the minimum of the first excited state or a crossing to the ground state is reached. The method is also of limited utility when states with strong double-excitation character are in play. On the other hand, ADC(2) dynamics (and, in a similar sense, TDDFT with a proper functional) should be particularly suitable when dynamical processes occurring within the excited-state manifold are of interest (e.g., exciton dynamics,[50] energy or electron transfer,[15] excimer formation,[51] and excited-state proton transfer[52]).

9H-Adenine in the gas phase, for which experimental data and simulated dynamics at various levels are available, was taken as a test case. The deactivation to the ground state predicted by ADC(2) is qualitatively correct, but somewhat smaller than the experimental result. As the present example of adenine shows, the ADC(2) method has been proven to be a very viable candidate in performing photodynamics simulations under the conditions discussed above. The present TDDFT results failed to predict the ultrafast deactivation of 9H-adenine, which is consistent with previous TDDFT simulations.[3]

A long-standing problem in dynamics of 9H-adenine is the role of each region of the intersection seam for internal conversion. ADC(2) dynamics predicted that conical intersections with C2 deformations are the main deactivation channel in the dynamics starting in the low-energy region of the spectrum. Intersections with C6 deformations are relevant as well, and its importance tends to increase for absorption in the high-energy part of the spectrum. Intersections due to H elimination play only a minor role.

Based on these results for adenine, we conclude that surface hopping with ADC(2) has a great potential as a single-reference method to provide high-level information on nonadiabatic processes involving multiple excited states. However, it will require more investigations to prove the generally excellent performance of ADC(2).

AUTHOR INFORMATION

Corresponding Authors

*E-mail: felix.plasser@iwr.uni-heidelberg.de (F.P.).
*E-mail: barbatti@kofo.mpg.de (M.B.).

Present Address

[○]Department of Chemistry, University of Bath, Claverton Down, BA2 7AY−Bath, U.K.

Notes

The authors declare no competing financial interest.

ACKNOWLEDGMENTS

F.P. is a recipient of a fellowship for postdoctoral researchers by the Alexander von Humboldt foundation. J.P. and M.P. acknowledge the support by the Grant Agency of Czech Republic (Project No. 208/12/0559). Support by the National Science Foundation (under Project No. CHE-1213263) and by the Robert A. Welch Foundation (under Grant No. D-0005) is also acknowledged. Computer time at the Vienna Scientific Cluster (Project No. 70019) is gratefully acknowledged.

REFERENCES

(1) (a) Barbatti, M. Nonadiabatic dynamics with trajectory surface hopping method. *WIREs: Comput. Mol. Sci.* **2011**, *1*, 620−633. (b) Tully, J. C. Molecular-Dynamics with Electronic-Transitions. *J. Chem. Phys.* **1990**, *93*, 1061−1071.

(2) Nelson, T.; Fernandez-Alberti, S.; Chernyak, V.; Roitberg, A. E.; Tretiak, S. Nonadiabatic excited-state molecular dynamics: Numerical tests of convergence and parameters. *J. Chem. Phys.* **2012**, *136*, 054108.

(3) Barbatti, M.; Lan, Z.; Crespo-Otero, R.; Szymczak, J. J.; Lischka, H.; Thiel, W. Critical appraisal of excited state nonadiabatic dynamics simulations of 9H-adenine. *J. Chem. Phys.* **2012**, *137*, 22A503.

(4) (a) Bonačić-Koutecký, V.; Mitrić, R. Theoretical exploration of ultrafast dynamics in atomic clusters: Analysis and control. *Chem. Rev.* **2005**, *105*, 11−65. (b) Tapavicza, E.; Meyer, A. M.; Furche, F. Unravelling the details of vitamin D photosynthesis by non-adiabatic molecular dynamics simulations. *Phys. Chem. Chem. Phys.* **2011**, *13*, 20986−20998. (c) Curchod, B. F. E.; Rothlisberger, U.; Tavernelli, I. Trajectory-Based Nonadiabatic Dynamics with Time-Dependent Density Functional Theory. *ChemPhysChem* **2013**, *14*, 1314−1340.

(5) (a) Christiansen, O.; Koch, H.; Jorgensen, P. The 2nd-Order Approximate Coupled-Cluster Singles and Doubles Model CC2. *Chem. Phys. Lett.* **1995**, *243*, 409−418. (b) Hättig, C.; Weigend, F. CC2 excitation energy calculations on large molecules using the resolution of the identity approximation. *J. Chem. Phys.* **2000**, *113*, 5154−5161. (c) Hättig, C.; Köhn, A. Transition moments and excited-state first-order properties in the coupled-cluster model CC2 using the resolution-of-the-identity approximation. *J. Chem. Phys.* **2002**, *117*, 6939−6951.

(6) (a) Schirmer, J. Beyond the random-phase approximation: A new approximation scheme for the polarization propagator. *Phys. Rev. A* **1982**, *26*, 2395−2416. (b) Trofimov, A. B.; Schirmer, J. An efficient polarization propagator approach to valence electron excitation spectra. *J. Phys. B: At., Mol. Opt. Phys.* **1995**, *28*, 2299−2324.

(7) (a) Barbatti, M.; Granucci, G.; Ruckenbauer, M.; Plasser, F.; Crespo-Otero, R.; Pittner, J.; Persico, M.; Lischka, H., *NEWTON-X: A package for Newtonian dynamics close to the crossing seam*. Available via the Internet at www.newtonx.org, 2013. (b) Barbatti, M.; Ruckenbauer, M.; Plasser, F.; Pittner, J.; Granucci, G.; Persico, M.; Lischka, H. Newton-X: A surface-hopping program for nonadiabatic molecular dynamics. *WIREs: Comput. Mol. Sci.* **2014**, *4*, 26−33.

(8) Ahlrichs, R.; Bär, M.; Häser, M.; Horn, H.; Kölmel, C. Electronic-Structure Calculations on Workstation Computers—The Program System Turbomole. *Chem. Phys. Lett.* **1989**, *162*, 165−169.

(9) Frisch, M. J.; Trucks, G. W.; Schlegel, H. B.; Scuseria, G. E.; Robb, M. A.; Cheeseman, J. R.; Scalmani, G.; Barone, V.; Mennucci, B.; Petersson, G. A.; Nakatsuji, H.; Caricato, M.; Li, X.; Hratchian, H.

P.; Izmaylov, A. F.; Bloino, J.; Zheng, G.; Sonnenberg, J. L.; Hada, M.; Ehara, M.; Toyota, K.; Fukuda, R.; Hasegawa, J.; Ishida, M.; Nakajima, T.; Honda, Y.; Kitao, O.; Nakai, H.; Vreven, T.; Montgomery, J., J., A.; Peralta, J. E.; Ogliaro, F.; Bearpark, M.; Heyd, J. J.; Brothers, E.; Kudin, K. N.; Staroverov, V. N.; Kobayashi, R.; Normand, J.; Raghavachari, K.; Rendell, A.; Burant, J. C.; Iyengar, S. S.; Tomasi, J.; Cossi, M.; Rega, N.; Millam, N. J.; Klene, M.; Knox, J. E.; Cross, J. B.; Bakken, V.; Adamo, C.; Jaramillo, J.; Gomperts, R.; Stratmann, R. E.; Yazyev, O.; Austin, A. J.; Cammi, R.; Pomelli, C.; Ochterski, J. W.; Martin, R. L.; Morokuma, K.; Zakrzewski, V. G.; Voth, G. A.; Salvador, P.; Dannenberg, J. J.; Dapprich, S.; Daniels, A. D.; Farkas, Ö.; Foresman, J. B.; Ortiz, J. V.; Cioslowski, J.; Fox, D. J. *Gaussian 09, Revision D.01*; Gaussian, Inc.: Wallingford, CT, 2013.

(10) Chai, J.-D.; Head-Gordon, M. Systematic optimization of long-range corrected hybrid density functionals. *J. Chem. Phys.* **2008**, *128*, 084106.

(11) Hirata, S.; Head-Gordon, M. Time-dependent density functional theory within the Tamm−Dancoff approximation. *Chem. Phys. Lett.* **1999**, *314*, 291−299.

(12) (a) Christiansen, O. First-order nonadiabatic coupling matrix elements using coupled cluster methods. I. Theory. *J. Chem. Phys.* **1999**, *110*, 711−723. (b) Ichino, T.; Gauss, J.; Stanton, J. F. Quasidiabatic states described by coupled-cluster theory. *J. Chem. Phys.* **2009**, *130*, 174105. (c) Tajti, A.; Szalay, P. G. Analytic evaluation of the nonadiabatic coupling vector between excited states using equation-of-motion coupled-cluster theory. *J. Chem. Phys.* **2009**, *131*, 124104.

(13) Hammes-Schiffer, S.; Tully, J. C. Proton-Transfer in Solution—Molecular-Dynamics with Quantum Transitions. *J. Chem. Phys.* **1994**, *101*, 4657−4667.

(14) Granucci, G.; Persico, M.; Toniolo, A. Direct semiclassical simulation of photochemical processes with semiempirical wave functions. *J. Chem. Phys.* **2001**, *114*, 10608.

(15) Plasser, F.; Granucci, G.; Pittner, J.; Barbatti, M.; Persico, M.; Lischka, H. Surface hopping dynamics using a locally diabatic formalism: Charge transfer in the ethylene dimer cation and excited state dynamics in the 2-pyridone dimer. *J. Chem. Phys.* **2012**, *137*, 22A514.

(16) Barbatti, M.; Lischka, H. Nonadiabatic Deactivation of 9H-Adenine: A Comprehensive Picture Based on Mixed Quantum-Classical Dynamics. *J. Am. Chem. Soc.* **2008**, *130*, 6831−6839.

(17) Fabiano, E.; Thiel, W. Nonradiative deexcitation dynamics of 9H-adenine: An OM2 surface hopping study. *J. Phys. Chem. A* **2008**, *112*, 6859−6863.

(18) Alexandrova, A. N.; Tully, J. C.; Granucci, G. Photochemistry of DNA Fragments via Semiclassical Nonadiabatic Dynamics. *J. Phys. Chem. B* **2010**, *114*, 12116−12128.

(19) Picconi, D.; Avila Ferrer, F. J.; Improta, R.; Lami, A.; Santoro, F. Quantum-classical effective-modes dynamics of the $\pi\pi^* \rightarrow n\pi^*$ decay in 9H-adenine. A quadratic vibronic coupling model. *Faraday Discuss.* **2013**, *163*, 223−242.

(20) (a) Lei, Y.; Yuan, S.; Dou, Y.; Wang, Y.; Wen, Z. Detailed Dynamics of the Nonradiative Deactivation of Adenine: A Semi-classical Dynamics Study. *J. Phys. Chem. A* **2008**, *112*, 8497−8504. (b) Mitrić, R.; Werner, U.; Wohlgemuth, M.; Seifert, G.; Bonačić-Koutecký, V. Nonadiabatic Dynamics within Time-Dependent Density Functional Tight Binding Method. *J. Phys. Chem. A* **2009**, *113*, 12700−12705.

(21) (a) Kang, H.; Jung, B.; Kim, S. K. Mechanism for ultrafast internal conversion of adenine. *J. Chem. Phys.* **2003**, *118*, 6717−6719. (b) Ullrich, S.; Schultz, T.; Zgierski, M. Z.; Stolow, A. Direct observation of electronic relaxation dynamics in adenine via time-resolved photoelectron spectroscopy. *J. Am. Chem. Soc.* **2004**, *126*, 2262−2263. (c) Canuel, C.; Mons, M.; Piuzzi, F.; Tardivel, B.; Dimicoli, I.; Elhanine, M. Excited states dynamics of DNA and RNA bases: Characterization of a stepwise deactivation pathway in the gas phase. *J. Chem. Phys.* **2005**, *122*, 074316. (d) Satzger, H.; Townsend, D.; Zgierski, M. Z.; Patchkovskii, S.; Ullrich, S.; Stolow, A. Primary processes underlying the photostability of isolated DNA bases: Adenine. *Proc. Natl. Acad. Sci. U.S.A.* **2006**, *103*, 10196−10201. (e) Evans, N. L.; Ullrich, S. Wavelength Dependence of Electronic Relaxation in Isolated Adenine Using UV Femtosecond Time-Resolved Photoelectron Spectroscopy. *J. Phys. Chem. A* **2010**, *114*, 11225−11230. (f) Kotur, M.; Weinacht, T. C.; Congyi, Z.; Matsika, S. Following Ultrafast Radiationless Relaxation Dynamics With Strong Field Dissociative Ionization: A Comparison Between Adenine, Uracil, and Cytosine. *IEEE J. Sel. Top. Quant.* **2012**, *18*, 187−194.

(22) Granucci, G.; Persico, M. Critical appraisal of the fewest switches algorithm for surface hopping. *J. Chem. Phys.* **2007**, *126*, 134114.

(23) Casida, M. E.; Huix-Rotllant, M. Progress in Time-Dependent Density-Functional Theory. *Annu. Rev. Phys. Chem.* **2012**, *63*, 287−323.

(24) Hättig, C., Structure Optimizations for Excited States with Correlated Second-Order Methods: CC2 and ADC(2). In *Advances in Quantum Chemistry*, Vol. *50*; Jensen, H. J. Å., Ed.; Academic Press: New York, 2005; pp 37−60.

(25) (a) Tapavicza, E.; Tavernelli, I.; Rothlisberger, U. Trajectory surface hopping within linear response time-dependent density-functional theory. *Phys. Rev. Lett.* **2007**, *98*, 023001. (b) Mitric, R.; Werner, U.; Bonacic-Koutecky, V. Nonadiabatic dynamics and simulation of time resolved photoelectron spectra within time-dependent density functional theory: Ultrafast photoswitching in benzylideneaniline. *J. Chem. Phys.* **2008**, *129*, 9. (c) Barbatti, M.; Pittner, J.; Pederzoli, M.; Werner, U.; Mitric, R.; Bonacic-Koutecky, V.; Lischka, H. Non-adiabatic dynamics of pyrrole: Dependence of deactivation mechanisms on the excitation energy. *Chem. Phys.* **2010**, *375*, 26−34.

(26) Casida, M., Time-dependent density functional response theory for molecules. In *Recent advances in density functional methods, Part I*; Chong, D., Ed.; World Scientific: Singapore, 1995; pp 155−192.

(27) Pittner, J.; Lischka, H.; Barbatti, M. Optimization of mixed quantum-classical dynamics: Time-derivative coupling terms and selected couplings. *Chem. Phys.* **2009**, *356*, 147−152.

(28) Crespo-Otero, R.; Barbatti, M. Spectrum simulation and decomposition with nuclear ensemble: formal derivation and application to benzene, furan and 2-phenylfuran. *Theor. Chem. Acc.* **2012**, *131*, 1237.

(29) Chai, J.-D.; Head-Gordon, M. Long-range corrected hybrid density functionals with damped atom−atom dispersion corrections. *Phys. Chem. Chem. Phys.* **2008**, *10*, 6615−6620.

(30) Dunning, T. H. Gaussian-Basis Sets for Use in Correlated Molecular Calculations. 1. The Atoms Boron through Neon and Hydrogen. *J. Chem. Phys.* **1989**, *90*, 1007−1023.

(31) (a) Lischka, H.; Muller, T.; Szalay, P. G.; Shavitt, I.; Pitzer, R. M.; Shepard, R. COLUMBUS—A program system for advanced multireference theory calculations. *Wiley Interdiscip. Rev.—Comput. Mol. Sci.* **2011**, *1*, 191−199. (b) Lischka, H.; Shepard, R.; Shavitt, I.; Pitzer, R. M.; Dallos, M.; Müller, T.; Szalay, P. G.; Brown, F. B.; Ahlrichs, R.; Böhm, H. J.; Chang, A.; Comeau, D. C.; Gdanitz, R.; Dachsel, H.; Ehrhardt, C.; Ernzerhof, M.; Höchtl, P.; Irle, S.; Kedziora, G.; Kovar, T.; Parasuk, V.; Pepper, M. J. M.; Scharf, P.; Schiffer, H.; Schindler, M.; Schüler, M.; Seth, M.; Stahlberg, E. A.; Zhao, J.-G.; Yabushita, S.; Zhang, Z.; Barbatti, M.; Matsika, S.; Schuurmann, M.; Yarkony, D. R.; Brozell, S. R.; Beck, E. V.; Blaudeau, J.-P.; Ruckenbauer, M.; Sellner, B.; Plasser, F.; Szymczak, J. J. *COLUMBUS, An Ab Initio Electronic Structure Program*, Release 7.0. Available via the Internet at www.univie.ac.at/columbus, 2012.

(32) Barbatti, M.; Ullrich, S. Ionization potentials of adenine along the internal conversion pathways. *Phys. Chem. Chem. Phys.* **2011**, *13*, 15492−15500.

(33) (a) Clark, L. B.; Peschel, G. G.; Tinoco, I. Vapor Spectra and Heats of Vaporization of Some Purine and Pyrimidine Bases. *J. Phys. Chem.* **1965**, *69*, 3615−3618. (b) Li, L.; Lubman, D. M. Ultraviolet Visible Absorption-Spectra of Biological Molecules in the Gas-Phase Using Pulsed Laser-Induced Volatilization Enhancement in a Diode-Array Spectrophotometer. *Anal. Chem.* **1987**, *59*, 2538−2541.

(34) Fleig, T.; Knecht, S.; Hättig, C. Quantum-chemical investigation of the structures and electronic spectra of the nucleic acid bases at the coupled cluster CC2 level. *J. Phys. Chem. A* **2007**, *111*, 5482−5491.
(35) Szalay, P. G.; Watson, T.; Perera, A.; Lotrich, V. F.; Bartlett, R. J. Benchmark Studies on the Building Blocks of DNA. 1. Superiority of Coupled Cluster Methods in Describing the Excited States of Nucleobases in the Franck−Condon Region. *J. Phys. Chem. A* **2012**, *116*, 6702−6710.
(36) Daniels, M.; Hauswirth, W. Fluorescence of the Purine and Pyrimidine Bases of the Nucleic Acids in Neutral Aqueous Solution at 300°K. *Science* **1971**, *171*, 675−677.
(37) Engler, G.; Seefeld, K.; Schmitt, M.; Tatchen, J.; Grotkopp, O.; Muller, T. J. J.; Kleinermanns, K. Acetylation makes the difference: A joint experimental and theoretical study on low-lying electronically excited states of 9H-adenine and 9-acetyladenine. *Phys. Chem. Chem. Phys.* **2013**, *15*, 1025−1031.
(38) Nir, E.; Plutzer, C.; Kleinermanns, K.; de Vries, M. Properties of isolated DNA bases, base pairs and nucleosides examined by laser spectroscopy. *Eur. Phys. J. D* **2002**, *20*, 317−329.
(39) Serrano-Andrés, L.; Merchán, M.; Borin, A. C. A three-state model for the photophysics of adenine. *Chem.—Eur. J.* **2006**, *12*, 6559−6571.
(40) Middleton, C. T.; de La Harpe, K.; Su, C.; Law, Y. K.; Crespo-Hernandez, C. E.; Kohler, B. DNA Excited-State Dynamics: From Single Bases to the Double Helix. *Annu. Rev. Phys. Chem.* **2009**, *60*, 217−239.
(41) Send, R.; Kaila, V. R. I.; Sundholm, D. Reduction of the virtual space for coupled-cluster excitation energies of large molecules and embedded systems. *J. Chem. Phys.* **2011**, *134*, 214114.
(42) (a) Janssen, C. L.; Nielsen, I. M. B. New diagnostics for coupled-cluster and Møller−Plesset perturbation theory. *Chem. Phys. Lett.* **1998**, *290*, 423−430. (b) Nielsen, I. M. B.; Janssen, C. L. Double-substitution-based diagnostics for coupled-cluster and Møller−Plesset perturbation theory. *Chem. Phys. Lett.* **1999**, *310*, 568−576.
(43) Köhn, A.; Hättig, C. Analytic gradients for excited states in the coupled-cluster model CC2 employing the resolution-of-the-identity approximation. *J. Chem. Phys.* **2003**, *119*, 5021−5036.
(44) Levine, B. G.; Ko, C.; Quenneville, J.; Martínez, T. J. Conical intersections and double excitations in time-dependent density functional theory. *Mol. Phys.* **2006**, *104*, 1039−1051.
(45) Lischka, H.; Dallos, M.; Szalay, P. G.; Yarkony, D. R.; Shepard, R. Analytic evaluation of nonadiabatic coupling terms at the MR-CI level. I. Formalism. *J. Chem. Phys.* **2004**, *120*, 7322−7329.
(46) Devore, J. L. *Probability & Statistics for Engineering and the Sciences*, 8th Edition; Cengage Learning: Stamford, CT, 2012; p 768.
(47) Cremer, D.; Pople, J. A. General Definition of Ring Puckering Coordinates. *J. Am. Chem. Soc.* **1975**, *97*, 1354−1358.
(48) Boeyens, J. C. A. The conformation of six-membered rings. *J. Chem. Crystallogr.* **1978**, *8*, 317−320.
(49) Fogarasi, G.; Zhou, X. F.; Taylor, P. W.; Pulay, P. The Calculation of Abinitio Molecular Geometries—Efficient Optimization by Natural Internal Coordinates and Empirical Correction by Offset Forces. *J. Am. Chem. Soc.* **1992**, *114*, 8191−8201.
(50) Bittner, E. R. Frenkel exciton model of ultrafast excited state dynamics in AT DNA double helices. *J. Photochem. Photobiol. A* **2007**, *190*, 328−334.
(51) Plasser, F.; Lischka, H. Electronic excitation and structural relaxation of the adenine dinucleotide in gas phase and solution. *Photochem. Photobiol. Sci.* **2013**, *12*, 1440−1452.
(52) Plasser, F.; Barbatti, M.; Aquino, A. J. A.; Lischka, H. Excited-State Diproton Transfer in [2,2′-Bipyridyl]-3,3′-diol: The Mechanism Is Sequential, Not Concerted. *J. Phys. Chem. A* **2009**, *113*, 8490−8499.